

Layered Hydride CaNiGeH with a ZrCuSiAs-type Structure: Crystal Structure, Chemical Bonding, and Magnetism Induced by Mn Doping

Xiaofeng Liu,^{†,⊥} Satoru Matsuishi,[‡] Satoru Fujitsu,[†] Toru Ishigaki,[§] Takashi Kamiyama,^{||} and Hideo Hosono^{*,†,‡}

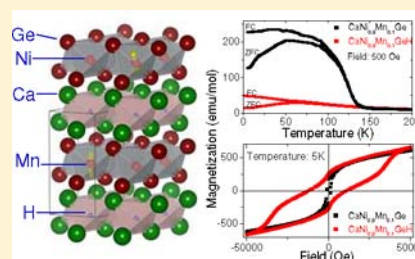
[†]Frontier Research Center, and [‡]Materials and Structures Laboratory, Tokyo Institute of Technology, 4259 Nagatsuta, Midori, Yokohama 226-8503, Japan

[§]Frontier Research Center for Applied Sciences, Ibaraki University, 162-1, Shirakata, Tokai, Naka, Ibaraki 319-1106, Japan

^{||}High Energy Accelerator Research Organization (KEK), Tsukuba, Ibaraki, 305-0801, Japan

Supporting Information

ABSTRACT: Stimulated by the discovery of the iron oxypnictide superconductor with ZrCuSiAs-type structure in 2008, extensive exploration of its isostructural and isoelectronic compounds has started. These compounds, including oxides, fluorides, and hydrides, can all be simply recognized as valence compounds for which the octet rule is valid. We report herein the first example of a ZrCuSiAs-type hydride, CaNiGeH, which violates the octet rule. This hydride was synthesized by hydrogenation of the CeFeSi-type compound CaNiGe under pressurized hydrogen. Powder diffraction and theoretical simulation confirm that H enters into the interstitial position of the Ca₄ tetrahedron, leading to notable anisotropic expansion of the unit cell along the *c* axis. Density functional theory calculations indicate the modification of the chemical bonding and formation of ionic Ca–H bond as a result of hydrogen insertion. Furthermore, CaNiGeH shows Pauli paramagnetism and metallic conduction similar to that of CaNiGe, but its carrier type changes to hole and the carrier density is drastically reduced as compared to CaNiGe. Mn-doping at the Ni site introduces magnetism to both the parent compound and the hydride. The measurement demonstrates that hydrogenation of CaNi_{1-x}Mn_xGe reduces ferromagnetic ordering of Mn ions and induces huge magnetic hysteresis, whereas the spin glass state observed for the parent compound is preserved in the hydride. The hydrogenation-induced changes in the electric and magnetic properties are interpreted in terms of development of two-dimensionality in crystal structure as well as electronic state.



1. INTRODUCTION

Compounds with the two-dimensional (2D) ZrCuSiAs-type (1111) and related structures have become of particular interest due to the discovery of the F-doped LaFeAsO superconductor in early 2008.^{1–3} This 1111-type structure with the formula of RTAB is built up from alternating layers of edge-sharing R₄ tetrahedrons [R: rare earth (Re) or alkali earth (Ae) elements] filled with B atoms (B: small anions such as O²⁻, F⁻, or H⁻) and A₄ tetrahedrons (A: group IV, V, or VI elements) filled with T atoms (T: transition metal).⁴ The common feature possessed by most of these quaternary compounds, including oxide, fluoride, and hydride, is that they all can be regarded as valence compounds because the octet rule is obeyed by simply assigning integer oxidation state for each constituent atom (e.g., La³⁺Fe²⁺As³⁻O²⁻).

The octet rule is, however, not always valid for the ternary CeFeSi-type (111) compounds (formulated by RTA), which can be viewed as an “unfilled” ZrCuSiAs-type structure.^{5–7} Because of the absence of the B atoms in the R₄ tetrahedrons, these compounds are always not electronically balanced. For instance, the Re-based 111-type compounds are expressed in the form of Re³⁺T²⁺X⁴⁻·e⁻ (X: Si or Ge). The excess electrons can be consumed by insertion of H into the Re₄ tetrahedron,

leading to ReTXH,^{8–10} where H is negatively charged and thus serves as the electron sink. For the case of Ae-based 111-type compounds, such as AeTGe (Ae = Mg, Ca, Sr, and Ba; T = Mn, Fe, Co, and Ni),^{11–13} the octet rule is already obeyed as they are electronically balanced. In this respect, the exploration of the hydride for these Ae-based compounds will provide new insight into the understanding of hydrogenation behavior and coordination for hydrogen in these systems.

After hydrogenation, the initial crystal of structure of the “111” is almost preserved in the “1111” type hydride, despite the anisotropic expansion of the unit cell. These systems could be therefore ideal platforms for studying the hydrogenation effect on the crystallographic, magnetic, and transport properties. Besides geometrical change, hydrogenation in general causes localization of conducting electrons at the negatively charged H ions, and hence the electric resistance notably increases as compared to their parent compounds. On the contrary, we cannot generalize the hydrogenation effect on the magnetic behavior. From a general perspective, hydrogen insertion into the R₄ tetrahedrons of the ReTX compounds

Received: March 17, 2012

Published: June 29, 2012

leads to the weakening of magnetic interaction for Re, which bonds exclusively to H. However, the change of magnetism in fact varies depending upon the nature of each compound and the magnetic ions. Chevalier et al. reported that hydrogenation triggered transition from antiferromagnetic (AFM) to spin fluctuation for CeCoSi(Ge),^{14,15} from heavy fermion to AFM for CeRuSi,¹⁶ and from AFM to ferromagnetic (FM) for NdCoSi.¹⁷ Hydrogenation also affects the magnetism of transition metal that does not bond directly to hydrogen. As Mn is always magnetically ordered in these compounds, NdMnSi was studied by the same author, and a weakening of AFM interaction for Mn in NdMnSiH as compared to NdMnSi was unraveled.¹⁸ The origin of these changes in the magnetic properties upon hydrogenation can be rationalized with the synergistic influence of geometric and electronic factors.¹⁹

Back to the AeTX compound, it has been well established that FM metals including Fe, Co, and Ni are nonmagnetic in these compounds, while the Mn always carry a local magnetic moment, leading to either FM or AFM ordering depending on the strength of exchange interaction, which is similar to the case of ReTX.^{11,20,21} However, our understanding on their interaction with hydrogen and the physical properties is far from sufficient as compared to their Re-based counterparts. In our previous work, Mn was chosen as the spin dopant to CaNiGe, and it was revealed that the system evolved from the Pauli paramagnetic (PPM) to FM and finally to a spin-glass (SG)-like state upon cooling.²² Hydrogenation, however, may provide new possibilities for the modification of magnetism in this system. During our exploration of hydride of the AeTX system, CaNiGeH was successfully obtained and confirmed with 1111-type structure (see Figure 1), while hydrogenation of

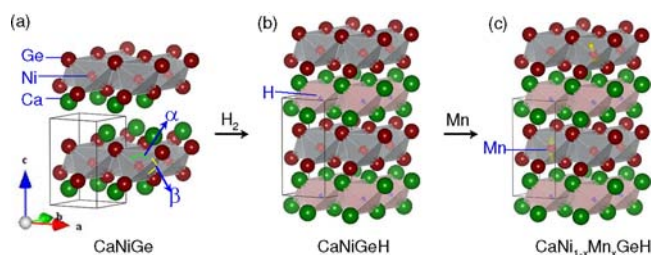


Figure 1. Crystal structure of (a) the parent compound CaNiGe with the CeFeSi-type structure, (b) the hydride CaNiGeH with the ZrCuSiAs-type structure, and (c) the magnetic hydride CaNi_{1-x}Mn_xGeH after spin injection by Mn doping at the Ni site. The 2-fold and 4-fold Ge–Fe–Ge bonding angles are designated as α and β , respectively.

CaMnGe and MgTGe (T: Mn, Fe, and Co) did not lead to single phase hydride. Here, in this Article, we present the structure and chemical bonding for the nonvalence compound CaNiGeH. Experiment combined with theoretical calculations point out that hydrogen atoms enter into the Ca₄ tetrahedrons of CaNiGe, leading to ionic Ca–H bonding and a notable increase in electric resistivity. Furthermore, hydrogen insertion in the Mn-doped CaNiGe removes FM ordering of Mn and induces huge magnetic hysteresis. The observed results are explained in terms of electron localization and the development of 2D crystal and electronic structures.

2. EXPERIMENTAL SECTION

Sample Synthesis. The parent compounds of CaNi_{1-x}Mn_xGe were synthesized by arc-melting from Ca, Ni, Mn, and Ge (purity 4 N)

grains. For each batch, the amount of Ca was in excess by 5% as compared to the stoichiometric ratio to compensate its evaporation loss during melting. The as-melted metallic ingots were crushed into fine particles, and then loaded into a tube furnace filled with 2.0 MPa H₂, where the samples were allowed for hydrogenation at 573 K for durations up to 40 h. After hydrogenation, the samples were pulverized into fine powders due to the large volume expansion as a result of hydrogenation. Analogously, CaNiGeD was synthesized under the same temperature and pressure conditions in the atmosphere of D₂.

Structural Characterization. The stoichiometry of H in the compounds CaNi_{1-x}Mn_xGeH were determined by thermogravimetry/mass spectroscopy (TG-MS) using a Bruker AXS TG-DTA/MS9610 system. The samples were heated from room temperature to 900 at 20 °C/min under a continuous argon flow, and the evolution of hydrogen from the sample was monitored by mass spectrum. Powder X-ray diffraction (XRD) pattern was collected with a Bruker D8 Advance diffractometer equipped with Cu K α radiation operating at 45 kV and 360 mA under ambient conditions. The XRD pattern can be unambiguously indexed with the *P4/nmm* structure, and it was further analyzed by Rietveld method using the EXPGUI-GSAS program.²³ To initialize the refinement, we adopted the structural model of the ZrCuSiAs-type compound SrFeAsF,^{24–26} where Ca, Ni(Mn), Ge, and H occupy the corresponding Sr(2c), Fe(2b), As(2c), and F(2b) sites in SrFeAsF. Peak profile and the background were described with the pseudo-Voigt function and the shifted Chebyshev polynomial, respectively. The March–Dollase function was employed to describe the observed strong preferred orientation along the [001] direction.^{27,28} The refined crystal structures are visualized using software VESTA.²⁹ Neutron powder diffraction (NPD) data for CaNiGeD was taken using a high throughput neutron diffractometer, iMATERIA, at the Japanese Particle Accelerator Research Complex (J-PARC).³⁰ The measurement time for data collection in the 0.2MW beam power was about 4 hours for 2.4 g powder sample contained in a 6 mm diameter cylindrical vanadium cell. Rietveld refinement for time-of-flight neutron powder diffraction data was performed using the program Z-Rietveld.^{31,32}

Physical Property Measurements. The powders of hydride were pressed into high-density pellets, and then cut into rectangular bars for resistivity measurement using a Quantum Design (QD) Physical Property Measurement System (PPMS) by the conventional four-probe method. Magnetism measurement was performed for particulate samples using the QD Superconducting Quantum Interference Device (SQUID) equipped with a vibrating-sample magnetometer (VSM). The Seebeck coefficient was determined by measuring thermoelectric voltage between the two sides of the sample bar under temperature gradient ($\Delta T < 5$ °C) at room temperature (24 °C).

Calculation Details. Density functional theory (DFT) calculations were performed using the generalized gradient approximation (GGA) with Perdew–Burke–Ernzerhof (PBE) functional and the projected augmented plane wave method implemented in the Vienna ab initio simulation program (VASP).^{33–35} The lattice parameters and atomic positions were fully relaxed by a structural optimization procedure minimizing the total energy and force. A conventional cell containing two chemical formulas and $6 \times 6 \times 4$ Monkhorst–Pack grids of *k* points was used, and the plane-wave basis-set cutoff was set to 600 eV. The projected density of states (PDOS) of each atom for both the CaNiGe and the CaNiGeH were obtained by decomposing the charge density over the atom-centered spherical harmonics with the same Wigner–Seitz radius $r = (3V_{\text{cell}}(\text{CaNiGeH})/4\pi N)^{1/3} = 1.55$ Å, where V_{cell} and *N* are the unit-cell volume and the number of atoms in a unit cell, respectively.

3. RESULTS AND ANALYSIS

Hydrogenation Behavior. The interaction of CeFeSi-type AeTX compounds with pressurized hydrogen (2–4 MPa) is quite different from that of their Re-based counterparts ReTX, most of which form monohydrides upon hydrogenation. During our material exploration, we performed hydrogenation for several AeTGe compounds (Ae = Mg, Ca; T = Mn, Fe, Co,

Ni), and we found that only CaNiGe absorbs hydrogen to form the ZrCuSiAs-type hydride CaNiGeH. In contrast, annealing of CaMnGe in H₂ resulted in the formation of CaH₂ and CaMn₂Ge₂. Other AeTX compounds, such as MgTGe (T: Mn, Fe, Co), did not absorb hydrogen under the same condition. This difference in the hydrogenation behavior may correlate with the difference in the electron count and chemical bonding of different AeTX compounds.

In our previous study, we obtained the single phase of CaNi_{1-x}Mn_xGe in both the Ni-rich (0 ≤ x ≤ 0.10) and the Mn-rich (0.90 ≤ x ≤ 1.0) composition regions. Here, we find that single phase hydride of the compounds in the Ni-rich side can be synthesized through annealing in pressurized H₂, while hydrogenation of the Mn-rich compounds leads to the disproportionation reaction similar to the hydrogenation behavior of CaMnGe. To determine the stoichiometry of the obtained hydride, we recorded the TG-mass profile for the hydride. Our assumption of the formation of monohydride CaNiGeH is well supported by the total weight loss of 0.576% (theoretical value 0.58%) as observed from TG profile given in Figure 2. Similarly, the compound CaNiGeD obtained under

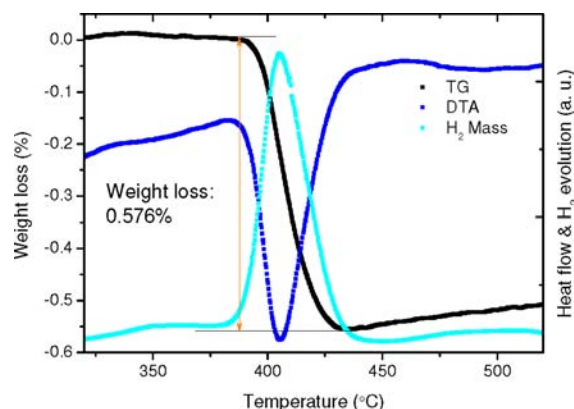


Figure 2. TG-DTA-mass profiles for CaNiGeH. An endothermic peak centered at 408 °C is observed from TG-DTA curves, which is associated with the evolution of gaseous hydrogen due to decomposition of the CaNiGeH as can be seen from the mass spectrum.

the same conditions shows a weight loss of 1.12%, which again confirms that the number of D (or H) atoms is the same as the number of Ca₄ tetrahedrons (and also number of Ca atoms) in the deuteride (or hydride). The decomposition of CaNiGeH begins from 370 °C and completes at 430 °C, as indicated by a sharp endothermic peak in the DSC curve and rapid hydrogen evolution in the mass spectrum. Further examination on CaNiGeH reveals that the hydrogenation process for CaNiGe is not reversible. The product after dehydrogenation contains Ca and CaNi₂Ge₂ (observed by XRD), and rehydrogenation of the sample under the same annealing condition leads to CaNi₂Ge₂, CaH₂, and a trace of NiGe_x alloy.

Crystal and Electronic Structure. The XRD pattern for the hydride CaNiGeH is shown in Figure 3a. Similar to its parent compounds, the hydride has the same 2D crystal structure as given in Figure 1, and therefore a strong preferred orientation along the [001] direction is observed. For the Rietveld fitting, the position of H atoms was fixed at the center of Ca₄ tetrahedron (1/4, 3/4, 0), and we found that the removal of all H atoms from the structure only shows a negligible influence on the result of fitting due to the small X-

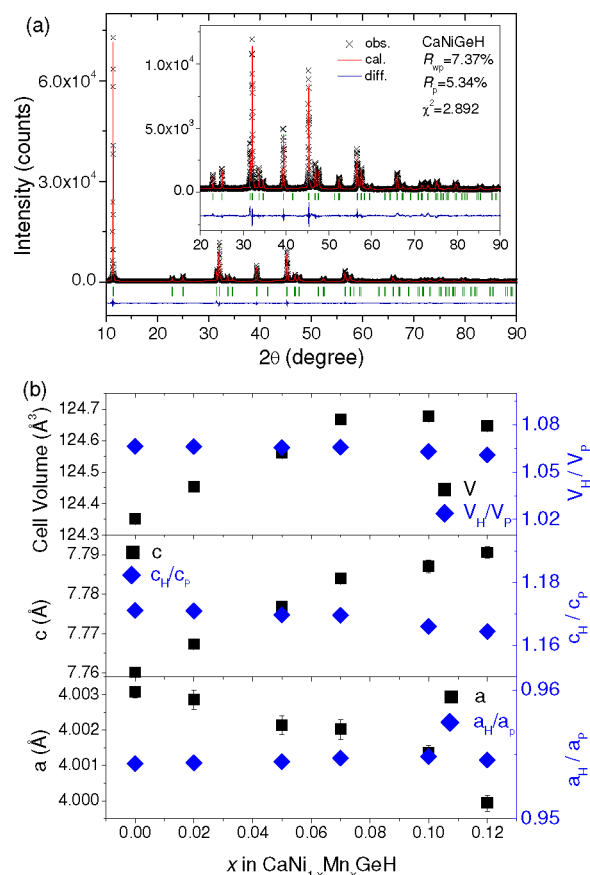


Figure 3. Structural characterization for CaNi_{1-x}Mn_xGeH by XRD. (a) XRD pattern together with Rietveld refinement for CaNiGeH. The insert shows the XRD pattern from 20° to 90°. (b) Dependence of lattice constants, cell volume, and the relative change of these structural parameters (defined as x_H/x_P , a , c , and V) for the hydrides with different Mn concentrations. The subscripts H and P represent the hydrides and the parent compounds, respectively.

ray scattering length of H atoms. To confirm the position of hydrogen, we performed NPD for the deuteride CaNiGeD. Figure S3 (in Supporting Information) shows the Rietveld refinement pattern of NPD for CaNiGeD. The result of NPD confirms that the D atoms enter into the Ca₄ tetrahedrons (Table S2). The structural model of hydrogen insertion is also supported by structural relaxation based on DFT calculations. The optimized lattice parameters a and c are 4.0010 and 7.7972 Å, respectively, which are very close to the experimental results. The obtained structural parameters and atomic coordinates are listed in Table 1. Similar to the structural evolution of CeFeSi upon hydrogenation,³⁶ the compound CaNiGe undergoes an overall cell volume expansion of 6.83%, together with a slight shrinkage along the a axis by 4.5%, and a notable stretching by 17.2% along the c direction (Figure 3b). In addition, hydrogen insertion also shifts the atomic coordinates along the c axis: Z_{Ca} varies from 0.1863 (in CaNiGe) to 0.1507, and Z_{Ge} from 0.6769 (in CaNiGe) to 0.6605. Through a closer comparison of the geometric change, it is clear that the Ca₄ tetrahedrons become smaller after hydrogen insertion, implying the formation of Ca–H bonding. The formation of Ca–H bond meanwhile weakens the bonds between Ca and Ge, and results in an increment of the Ca–Ge distance for the hydride as compared to the parent compound. Consequently, the NiGe₄ tetrahedrons are stretched along the c axis, and therefore the 2-

Table 1. Structure Parameters for CaNiGe and CaNiGeH from XRD Rietveld Refinement, and Simulated Results for CaNiGeH

formula	CaNiGeH	CaNiGe ¹¹	CaNiGeH ^a		
space group	<i>P4/nmm</i>	<i>P4/nmm</i>	<i>P4/nmm</i>		
<i>Z</i>	2	2	2		
<i>a</i> (Å)	4.0038(1)	4.19341(3)	4.00100		
<i>c</i> (Å)	7.7650(1)	6.6264(1)	7.79720		
cell volume (Å ³)	124.476	116.523(2)	124.817		
density (g/cm ³)	4.597	4.885	4.584		
<i>d</i> _{Ca–Ca} (Å)	3.67	3.780			
<i>d</i> _{Ca–Ge} (Å)	3.19	3.101			
<i>d</i> _{Ni–Ni} (Å)	2.83	2.965			
<i>d</i> _{Ni–Ge} (Å)	2.36	2.433			
$\alpha_{\text{Ge–Ni–Ge}}$ (deg) ^b	116.19	119.03			
$\beta_{\text{Ge–Ni–Ge}}$ (deg) ^c	106.22	104.92			
atom	site	<i>x</i>	<i>y</i>	<i>z</i>	<i>U</i> _{iso}
Ca	2c	1/4	1/4	0.1507(5)	0.042(3)
Ni	2b	3/4	1/4	1/2	0.033(1)
Ge	2c	1/4	1/4	0.6605(1)	0.039(1)
H	2a	3/4	1/4	0	0.050(1)

^aStructure parameters obtained from simulation. ^{b,c} α and β are the 2-fold and the 4-fold Ge–Ni–Ge bonding angle, respectively (see Figure 1).

fold Ge–Ni–Ge bond angle (α) decreases from 119.03° to 116.2°. These above results demonstrate the development of 2D structure by hydrogenation, reflected in the formation of the CaH and NiGe layers.

With an increment in the Mn concentration, the lattice parameter *c* increases, whereas *a* decreases. This behavior is consistent with the trend as observed in their parent compounds. However, the cell volume reaches a maximum of 124.7 Å³ at a solubility limit of *x* = 0.1, beyond which the cell volume decreases as the CaNi_{1–*x*}Mn_{*x*}Ge system probably undergoes cluster formation or phase separation. The relative change of lattice constants, defined as *a*_H/*a*_p (or *c*_H/*c*_p), remains almost unaffected at different levels of Mn doping (Figure 3b).

As compared to hydride, the deuteride CaNiGeD shows a slightly smaller unit cell (see Tables S1 and S2 in the Supporting Information). This result seems quite abnormal because the unit cells of deuteride are normally expanded as compared to those of hydrides. The structural difference between CaNiGeH and CaNiGeD is that the position of the Ca atom has been shifted along the *c* axis, and thus the bond length of Ca–H is shorter than that of Ca–D in CaNiGeD.

Figure 4 shows the band dispersion and the PDOS for CaNiGe and CaNiGeH calculated based on DFT. The DOS for CaNiGe is very similar to the results obtained by linear muffin-tin orbital (LMTO) method.¹² The observed metallic nature of the parent compound CaNiGe and its hydride is consistent with the presence of several bands that cross Fermi level and the absence of band gap in DOS. The DOS at *E*_f [*N*(*E*_f)] is slightly lowered after hydrogenation, which is in agreement with the results from transport measurements. Moreover, in CaNiGe, the atomic state of Ca contributes to the formation of conduction band, while in CaNiGeH the participation of the states of Ca and H is negligibly small, implying the reduction of metallic bonding to Ca. We have also calculated the Fermi surfaces (FS) for CaNiGe and CaNiGeH, as shown in Figure S6 in the Supporting Information. The FS is notably simplified after hydrogen insertion, and it is rather difficult to give a clear

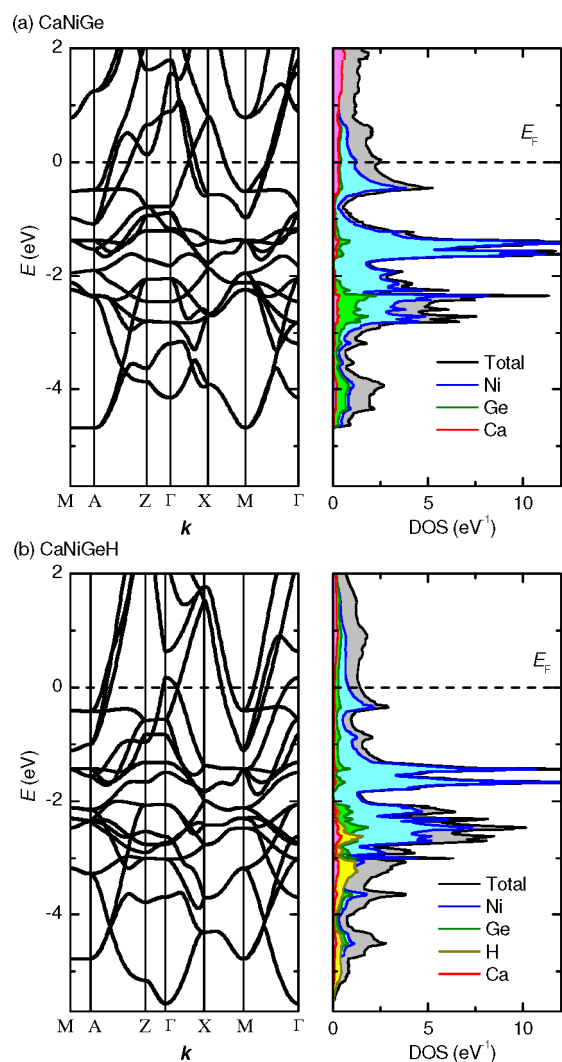


Figure 4. Band structure (right panel), and total DOS and PDOS (left panel) for (a) CaNiGe and (b) CaNiGeH. The Fermi level is set at 0 eV.

interpretation, while it is evident that a hole-like pocket is present for CaNiGeH, while it is absent for CaNiGe, reminiscent of a quasi 2D electronic/crystal structure.

DFT calculations and structural characterization have clarified that H enters into the Ca₄ tetrahedrons, leading to Ca–H bonding. By integrating the PDOS for the energy region from –12 eV to the Fermi level (0 eV), we may derive quantitatively the contribution of each atomic state for CaNiGe (Ca, 0.74; Ni, 10.28; and Ge, 3.58) and CaNiGeH (Ca, 0.69; Ni, 10.37; Ge, 3.62; and H, 1.75). The relative large decrease in the Ca state in the hydride indicates the formation of Ca–H bond. This is also reflected by a large contribution of the H 1s state, which suggests the localization of conduction electrons on H and the formation of hydrogen anion. As compared to Ca, Ni and Ge are almost not affected by hydrogenation due to the large distances between H and Ni (or Ge). A similar change in the electronic structure has also been observed after hydrogenation of the CeFeSi and CeScSi-type compounds, despite that the Re–H bond is in fact more covalent than the Ca–H bond.^{15,18,37,38}

Transport and Magnetic Properties. The electric resistance was measured with rectangular bars of compacted

powders. Because of the presence of considerable porosity, precise determination of the resistivity was not possible; however, the measurement clearly revealed an increase of resistivity for the hydrides by at least 2 orders of magnitude as compared to their parent compounds. This change can be understood in terms of electron localization on H due to the formation of ionic Ca–H bond. The increase in the resistivity, or even transformation from metallic to semiconducting, has been observed for the hydrides of many CeScSi-type and Zintl compounds.^{37,39} Figure 5 shows the normalized resistivity as a

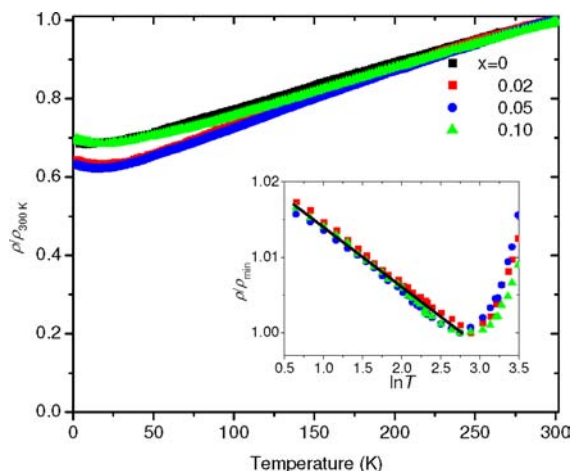


Figure 5. Normalized resistivity as a function of temperature for $\text{CaNi}_{1-x}\text{Mn}_x\text{GeH}$. The inset shows the normalized resistivity as a function of $\ln T$.

function of temperature recorded from 300 to 1.8 K. At high temperatures, the temperature dependence of resistivity for all of the examined samples exhibits good linearity, suggesting typical metallic conduction. With a decrease of temperature, ρ reaches minimum at around 20 K and then increases with a further decrease of temperature for the Mn-doped samples. The presence of a resistivity minimum at low temperatures and the linear-like dependence of resistance on $\ln T$ might possibly be attributed to Kondo-effect,⁴⁰ which stems from the scattering of the conducting electrons by the magnetic dopant of Mn.

The thermopower was measured to determine the type of charge carrier. It is revealed that the carrier type for the parent compound CaNiGe is electron as indicated by the negative thermopower (Seebeck coefficient α) of $-8.41 \mu\text{V/K}$. After hydrogen insertion, hole is the charge carrier, and the value increases to $20.04 \mu\text{V/K}$. The changing sign and increase in the thermal power strongly support the DFT calculation result that indicates the decrease in carrier density and the development of a hole-like pocket for CaNiGeH . The result further suggests the trapping of conduction electrons by H, leading to the negatively charged hydrogen anion.

Hydrogenation also exerts a huge influence on the magnetic behavior. Before presenting the magnetic measurement for the hydride, we need to point out here that both the parent compound and the hydride without Mn-doping show temperature-independent susceptibility, PPM. Moreover, to understand the magnetism of the hydride, we also need to recall the results as revealed by our previous study that the doping of Mn into the CaNiGe induces strong magnetic interaction into the system, resulting in the onset of FM ordering at around 120 K, followed by a magnetic glass transition at a lower temper-

ature.²² Figure 6a shows the temperature dependence of magnetization for the hydrides with different Mn concentrations. A small amount of paramagnetic impurity (probably due to NiGe_x alloys that also present in the parent compounds) contributes to the slight upturn of magnetization at temperature approaching zero, and this does not affect the following discussions. From the zero-field cooled (ZFC) and field-cooled (FC) curves, we can clearly observe that strong magnetic irreversibility occurs after the smooth increase of magnetization at around 20 and 80 K for $x = 0.05$ and 0.10, respectively. In contrast, magnetic irreversibility develops from around 200 K for $x = 0.02$. The same feature was also observed for its parent compounds ($\text{CaNi}_{0.98}\text{Mn}_{0.02}\text{Ge}$), and this can be attributed to a weak AFM ordering. For all of the studied Mn-doped hydrides, the weak anomaly located at approximately 70 K can be ascribed to AFM transition of Mn sublattice within the *ab* plane. Unlike the parent compounds, no observable FM transition is present for each of the hydrides examined, implying weakening of magnetic interaction after hydrogenation. However, the observation of bifurcation in the ZFC and FC curves can be still interpreted in terms of SG behavior due to competing AFM and FM interactions in this system.

Figure 6b shows the M – T curves for $\text{CaNi}_{0.9}\text{Mn}_{0.1}\text{Ge}$ measured at magnetic fields from 200 to 10 000 Oe. It becomes fairly clear that the magnetic glassy behavior is more pronounced at higher fields. This is not a feature observed for typical SG systems, in which the unparallel spins are often reoriented and the SG behavior is destroyed by the applied high field. This result suggests a noncanonical SG behavior, and the high magnetic hysteresis for this system implies strong FM interaction.

Unlike their parent compounds, before entering into the SG state, the hydrides do not exhibit characteristic paramagnetic behavior, and thus simple Curie–Weiss (C–W) law does not apply for all of the studied hydrides in the range from T_g (glass transition temperature) to 300 K. The deviation from C–W behavior at temperatures higher than T_g is often observed for SG systems,^{41,42} and it is in general associated with the presence of low-dimensional magnetic ordering, which could be triggered by hydrogenation for the present system. It has to be noted here that the system of $\text{CaNi}_{1-x}\text{Mn}_x\text{GeH}$ is situated near structural instability, and tends to compositional fluctuation or cluster formation that might be of AFM or FM character. These magnetic interactions present in the systems cause the non-C–W behavior at high temperatures and finally lead to SG at lower temperatures as we have observed by magnetization measurements.

Isothermal magnetization curves were recorded at 5, 25, 150, and 300 K for $\text{CaNi}_{1-x}\text{Mn}_x\text{GeH}$ ($x = 0.02, 0.05, \text{ and } 0.1$), as shown in Figure 6c. At room temperature, all of the hydrides with different compositions are in the paramagnetic state, while after entering into the glassy state the M – H curves become S-shaped, similar to their SG parent compounds. It seems quite interesting that magnetic hysteresis at 5 K increases rapidly with an increment of Mn-concentration, and a maxima coercive field of $H_c = 13.5 \text{ kOe}$ is observed for the sample $x = 0.1$ from the hysteresis loop given in Figure 6c, suggesting strong FM interaction. In addition, the maxima magnetic moments at 5 T are very close to results of the parent compounds. This result implies the presence of strong FM interaction for samples with high Mn concentration and points out that hydrogenation only leads to weakening of FM interaction, but does not change the character of SG behavior and the number of magnetic moment.

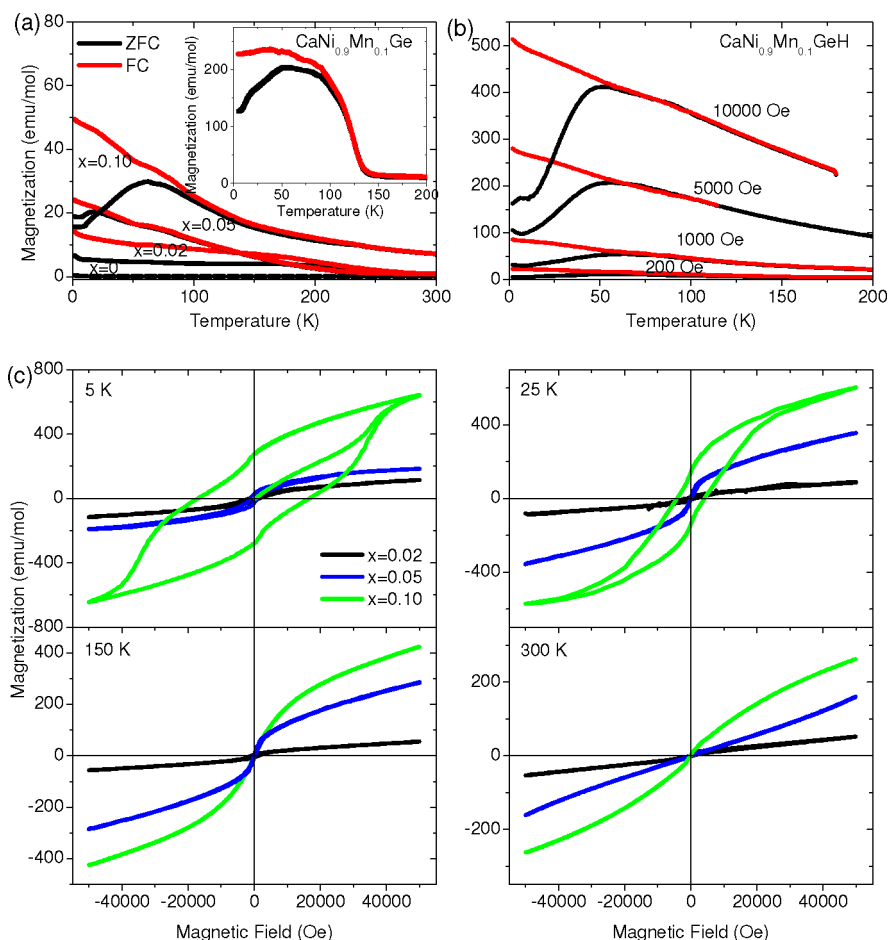


Figure 6. Magnetic properties of $\text{CaNi}_{1-x}\text{Mn}_x\text{GeH}$. (a) Temperature dependence of magnetization for the $\text{CaNi}_{1-x}\text{Mn}_x\text{GeH}$ measured at 500 Oe at ZFC and FC mode. The inset gives the M – T curves for $\text{CaNi}_{0.9}\text{Mn}_{0.1}\text{Ge}$ as a reference. (b) Temperature dependence of magnetization for $\text{CaNi}_{1-x}\text{Mn}_x\text{GeH}$ measured at magnetic fields from 200 to 10 000 Oe. (c) Isothermal magnetization curves recorded at temperatures of 5, 25, 150, and 300 K.

4. DISCUSSION

From crystal chemistry consideration, hydrogenation leads to the development of two-dimensionality in both crystal and electronic structure, resulting in the localization of conducting electrons on H^- . Similar to iron-based superconductors,³ the parent compound CaNiGe can be simply regarded as a valence compound in the form of $\text{Ca}^{2+}\text{Ni}^{2+}\text{Ge}^{4-}$, for which the octet rule is valid. It is, however, not appropriate from chemists' viewpoint because metallic bonding is present between Ca and NiGe layer and strong covalent and metallic bonding is involved for the NiGe layer as indicated by theoretical calculation. To reflect the ionic bonding character between Ca and NiGe layer, the compound CaNiGe should be better described as $\text{Ca}^{2+}(\text{NiGe})^{2-}$. After insertion of H, the octet rule is apparently not obeyed. Ca become more ionic, and each CaH pair is positively charged in the form of $[\text{CaH}]^+$; therefore, the hydride CaNiGeH can be viewed as $[\text{CaH}]^+[\text{NiGe}]^-$. It has to be pointed out here that the integer charge numbers assigned for individual atom (or atom pairs) do not represent real charges. These formulations, however, reflect the bonding character for both CaNiGe and CaNiGeH in a simplified manner, despite that the real charges carried by each pair could be far smaller because mixed bonding nature of these compounds.

Regarding magnetism, both CaNiGeH and CaNiGe are PPM due to electron itinerancy, and hence Ni in the hydride CaNiGeH does not carry a local magnetic moment. Similar to the parent compound, the observed magnetic behavior can be solely attributed to the magnetic dopant Mn. For Mn-based CeFeSi and ThCr_2Si_2 -type compounds, it has been generally accepted that the magnetic interaction between Mn ions varies from AFM, FM, to nonmagnetic (NM) depending upon the in-plane Mn–Mn distance.^{19,43} Therefore, the observed SG-like magnetic behavior can be interpreted in terms of competing AFM and FM interactions involving Mn ions distributed randomly in the 2D lattice. Because the system is metallic, the SG behavior probably stems from Ruderman–Kittel–Kasuya–Yosida (RKKY) interaction that is mediated by conduction electrons.^{44–46} After hydrogenation, the number of conduction electrons available for magnetic coupling through RKKY interaction is reduced as discussed previously, leading to the weakening of magnetic interaction. Besides the electronic factor, it has been observed that hydrogenation leads to the shrinkage of the unit cell within the ab plane, and hence the distance between two nearby Mn ions is reduced, which is also expected to affect magnetic interaction. However, the interplay of electronic and geometric factors on the magnetic behavior still needs to be elucidated in a more precise manner by further experiment.

The final remark concerns the magnetic hysteresis. For the system of $\text{CaNi}_{1-x}\text{Mn}_x\text{Ge}$, the origin of FM ordering is explained to correlate with FM cluster precipitated as a result of compositional fluctuation or phase separation as this system reaches solubility limit at $x = 0.1$.²² After hydrogenation, it is reasonable to consider that this kind of structural inhomogeneity is preserved. From a general viewpoint, the coercive force observed from the hysteresis loop for the hydride and the parent compounds could relate inherently with the crystal anisotropy, which impedes magnetization rotation with magnetic anisotropy.^{47,48} For the case of $\text{CaNi}_{0.9}\text{Mn}_{0.1}\text{GeH}$, the large magnetic hysteresis can be ascribed to the impeding of magnetization reversal or pinning of domain walls by structural defects or secondary phase precipitates,⁴⁹ which is induced by the tendency to structure instability for this composition. On the other hand, the sample of $\text{CaNi}_{0.9}\text{Mn}_{0.1}\text{GeH}$ behaves somewhat like a metamagnet as can be inferred from the double jumps in the $M-H$ curves in Figure 6.⁵⁰ This explanation is in line with the interpretation of the SG behavior originating from competing AFM and FM interaction. A high magnetic field induces spin flips in the AFM domains and hence leads to FM ordering of the spins through out the sample. The presence of such a field-induced magnetic transition inevitably results in the large magnetic hysteresis. Although the metamagnet is a convincing candidate to explain the large magnetic hysteresis, it is yet to be clarified by systematical investigation on the magnetization of this system.

5. SUMMARY

In the present work, we demonstrate that hydrogenation of the CeFeSi-type compound CaNiGe leads to the formation of the ZrCuSiAs-type hydride CaNiGeH , where H enters into the Ca_4 tetrahedron. It is revealed that hydrogen insertion induces notable anisotropic expansion along the c direction by 17%. Physical property measurements reveal that the hydride remains metallic and shows the same PPM as its parent compound, but the carrier density is drastically reduced and the carrier type changes to hole as compared to electron in the parent compound. With Mn-doping, hydrogenation exerts a remarkable influence on the magnetic behavior of Mn ions. FM ordering of Mn was removed after hydrogenation, whereas the SG behavior was almost preserved for the hydride. Hydrogenation also results in the large magnetic coercive force of hydride doped with high concentration of Mn ($x = 0.10$). These hydrogenation induced changes in the electro-magnetic properties are interpreted in terms of development of two-dimensionality in crystal structure as well as electronic state. The results of the present investigation suggest that hydrogenation could be an efficient method for the modification of electric and magnetic properties, implying potential application in electronics and spintronics. Furthermore, the modification of magnetism by hydrogenation may have implications in the design of FM materials with strong coercive force.

■ ASSOCIATED CONTENT

Supporting Information

XRD patterns for $\text{CaNi}_{1-x}\text{Mn}_x\text{H}$ ($x = 0.05$ and 0.1) and NPD pattern for CaNiGeD , CIF files for CaNiGeD and $\text{CaNi}_{1-x}\text{Mn}_x\text{H}$ ($x = 0.05$ and 0.1), and Fermi surfaces calculated for CaNiGe and CaNiGeH . This material is available free of charge via the Internet at <http://pubs.acs.org>.

■ AUTHOR INFORMATION

Corresponding Author

hosono@lucid.msl.titech.ac.jp

Present Address

¹Department of Colloid Chemistry, Max-Planck-Institute of Colloids and Interfaces, Research Campus Golm, 14424 Potsdam, Germany.

Notes

The authors declare no competing financial interest.

■ ACKNOWLEDGMENTS

This research was granted by the Japan Society for the Promotion of Science (JSPS) through the "Funding Program for World-Leading Innovative R&D on Science and Technology (FIRST Program)". We thank Dr. H. Mizoguchi for helping with the Seebeck coefficient measurement. X.L. thanks Dr. Yu Kang for stimulating discussions.

■ REFERENCES

- (1) Kamihara, Y.; Watanabe, T.; Hirano, M.; Hosono, H. *J. Am. Chem. Soc.* **2008**, *130*, 3296–3297.
- (2) Kamihara, Y.; Hiramatsu, H.; Hirano, M.; Kawamura, R.; Yanagi, H.; Kamiya, T.; Hosono, H. *J. Am. Chem. Soc.* **2006**, *128*, 10012–10013.
- (3) Johnston, D. C. *Adv. Phys.* **2010**, *59*, 803–1061.
- (4) Pöttgen, R.; Johrendt, D. *Z. Naturforsch., B* **2008**, *63*, 1135–1148.
- (5) Johnson, V.; Jeitschko, W. *J. Solid State Chem.* **1974**, *11*, 161–166.
- (6) Nieuwenkamp, W.; Bijvoet, J. M. *Z. Kristallogr., Kristallgeom., Kristallphys., Kristallchem.* **1932**, *81*, 469–474.
- (7) Pearson, W. B. *Z. Kristallogr.* **1985**, *171*, 23–39.
- (8) Chevalier, B.; Gaudin, E.; Geibel, C.; Canales, N. C.; Hermes, W.; Pöttgen, R. *J. Phys.: Condens. Matter* **2010**, *22*, 046003/1–046003/6.
- (9) Bobet, J. L.; Pasturel, M.; Chevalier, B. *Intermetallics* **2006**, *14*, 544–550.
- (10) Chevalier, B.; Matar, S. F.; Ménétrier, M.; Sanchez Marcos, J.; Fernandez, R. J. *J. Phys.: Condens. Matter* **2006**, *18*, 6045–6056.
- (11) Dascoulidou, A.; Schucht, F.; Jung, W.; Schuster, H. U. *Z. Anorg. Allg. Chem.* **1998**, *624*, 119–123.
- (12) Hlukhyy, V.; Chumalo, N.; Zaremba, V.; Fässler, T. F. *Z. Anorg. Allg. Chem.* **2008**, *634*, 1249–1255.
- (13) Welter, R.; Malaman, B.; Venturini, G. *Solid State Commun.* **1998**, *108*, 933–938.
- (14) Chevalier, B.; Matar, S. F. *Phys. Rev. B* **2004**, *70*, 174408/1–174408/9.
- (15) Chevalier, B.; Gaudin, E.; Weill, F.; Bobet, J. L. *Intermetallics* **2004**, *12*, 437–442.
- (16) Chevalier, B.; Gaudin, E.; Tencé, S.; Malaman, B.; Fernandez, J. R.; André, G.; Coqblin, B. *Phys. Rev. B* **2008**, *77*, 014414/1–014414/10.
- (17) Tencé, S.; Matar, S. F.; André, G.; Gaudin, E.; Chevalier, B. *Inorg. Chem.* **2010**, *49*, 4836–4842.
- (18) Tencé, S.; André, G.; Gaudin, E.; Bonville, P.; Al Alam, A. F.; Matar, S. F.; Hermes, W.; Pöttgen, R.; Chevalier, B. *J. Appl. Phys.* **2009**, *106*, 033910/1–033910/13.
- (19) Chevalier, B.; Tencé, S.; Gaudin, E.; Matar, S. F.; Bobet, J. L. *J. Alloys Compd.* **2009**, *480*, 43–45.
- (20) Dascoulidou, A.; Müller, P.; Bronger, W. *Z. Anorg. Allg. Chem.* **1998**, *624*, 124–128.
- (21) Welter, R.; Venturini, G.; Ressouche, E.; Malaman, B. *Solid State Commun.* **1996**, *97*, 503–507.
- (22) Liu, X.; Matsuishi, S.; Fujitsu, S.; Hosono, H. *Phys. Rev. B* **2011**, *84*, 214439/1–214439/6.
- (23) Toby, B. H. *J. Appl. Crystallogr.* **2001**, *34*, 210–213.
- (24) Matsuishi, S.; Inoue, Y.; Nomura, T.; Yanagi, H.; Hirano, M.; Hosono, H. *J. Am. Chem. Soc.* **2008**, *130*, 14428–14429.

- (25) Matsuishi, S.; Inoue, Y.; Nomura, T.; Hirano, M.; Hosono, H. *J. Phys. Soc. Jpn.* **2008**, *77*, 113709/1–113709/3.
- (26) Tegel, M.; Johansson, S.; Weiss, V.; Schellenberg, I.; Hermes, W.; Pöttgen, R.; Johrendt, D. *EPL* **2008**, *84*, 67007/1–67007/5.
- (27) March, A. Z. *Kristallogr.* **1932**, *81*, 285–297.
- (28) Dollase, W. A. *J. Appl. Crystallogr.* **1986**, *19*, 267–272.
- (29) Momma, K.; Izumi, F. *J. Appl. Crystallogr.* **2008**, *41*, 653–658.
- (30) Ishigaki, T.; Hoshikawa, A.; Yonemura, M.; Morishima, T.; Kamiyama, T.; Oishi, R.; Aizawa, K.; Sakuma, T.; Tomota, Y.; Arai, M.; Hayashi, M.; Ebata, K.; Takano, Y.; Komatsuzaki, K.; Asano, H.; Takano, Y.; Kasao, T. *Nucl. Instrum. Methods Phys. Res., Sect. A* **2009**, *600*, 189–191.
- (31) Oishi, R.; Yonemura, M.; Nishimaki, Y.; Torii, S.; Hoshikawa, A.; Ishigaki, T.; Morishima, T.; Mori, K.; Kamiyama, T. *Nucl. Instrum. Methods Phys. Res., Sect. A* **2009**, *600*, 94–96.
- (32) Oishi-Tomiyasu, R.; Yonemura, M.; Morishima, T.; Hoshikawa, A.; Torii, S.; Ishigaki, T.; Kamiyama, T. *J. Appl. Crystallogr.* **2012**, *45*, 299–308.
- (33) Perdew, J. P.; Burke, K.; Ernzerhof, M. *Phys. Rev. Lett.* **1996**, *77*, 3865–3868.
- (34) Blöchl, P. E. *Phys. Rev. B* **1994**, *50*, 17953–17979.
- (35) Kresse, G.; Furthmüller, J. *Phys. Rev. B* **1996**, *54*, 11169–11186.
- (36) Chevalier, B.; Pasturel, M.; Bobet, J. L.; Isnard, O. *Solid State Commun.* **2005**, *134*, 529–533.
- (37) Chevalier, B.; Hermes, W.; Heying, B.; Rodewald, U. C.; Hammerschmidt, A.; Matar, S. F.; Gaudin, E.; Pöttgen, R. *Chem. Mater.* **2010**, *22*, 5013–5021.
- (38) Gaudin, E.; Matar, S. F.; Pöttgen, R.; Eul, M.; Chevalier, B. *Inorg. Chem.* **2011**, *50*, 11046–11054.
- (39) Evans, M. J.; Holland, G. P.; Garcia-Garcia, F. J.; Häussermann, U. *J. Am. Chem. Soc.* **2008**, *130*, 12139–12147.
- (40) Kondo, J. *Prog. Theor. Phys.* **1964**, *32*, 37–49.
- (41) Lei, H.; Abeykoon, M.; Bozin, E. S.; Petrovic, C. *Phys. Rev. B* **2011**, *83*, 180503/1–180503/4.
- (42) Eriksson, T.; Nordblad, P.; Andersson, Y. *J. Solid State Chem.* **2005**, *178*, 1495–1502.
- (43) Dincer, I.; Elmali, A.; Elerman, Y.; Ehrenberg, H.; Fuess, H.; Daoud-Aladine, A. *J. Alloys Compd.* **2005**, *403*, 53–64 and references therein.
- (44) Ruderman, M. A.; Kittel, C. *Phys. Rev.* **1954**, *96*, 99–102.
- (45) Kasuya, T. *Prog. Theor. Phys.* **1956**, *16*, 45–57.
- (46) Yoshida, K. *Phys. Rev.* **1957**, *106*, 893–898.
- (47) Buschow, K. H. J.; de Boer, F. R. *Physics of Magnetism and Magnetic Materials*; Kluwer Academic Publishers: New York, 2003; p 112.
- (48) Givord, D.; Lu, O.; Rossignol, M. F.; Tenaud, P.; Viadieu, T. *J. Magn. Magn. Mater.* **1990**, *83*, 183–188.
- (49) Livingston, J. D. *J. Appl. Phys.* **1981**, *52*, 2544–2548.
- (50) Stryjewski, E.; Giordano, N. *Adv. Phys.* **1977**, *26*, 487–650.